Structural Biology: The State of the Art, ISBN 0-940030-42-X
Proceedings of the Eighth Conversation, State University of New York, Albany, NY 1993
Eds. Ramaswamy H. Sarma and Mukti H. Sarma, ©Adenine Press 1994

A Parallel-Stranded Double Helix at Atomic Resolution

Paolo Lubini and Martin Egli*
Organic Chemistry Laboratory
ETH Swiss Federal Institute of Technology
CH-8092 Zürich, Switzerland

Abstract

The X-ray crystal structure of a deoxycytidylyl-(3′-5′)-deoxycytidine dimer analogue containing intranucleosidyl C(3′)-C(5′) ethylene bridges was determined at a resolution of 1.0 Å. In the crystal, two dimers form a parallel-stranded, right-handed duplex, paired via hemiprotonated C-C^+ base pairs with three hydrogen bonds. In the duplex, base pairs are stacked at a distance of 3.44 Å with a helical twist of 34°. Dipole-dipole interactions between carbonyl groups from stacked cytosine bases and base stacking interactions contribute to the stability of the duplex. Sugar puckers and backbone torsion angles, except for β and γ, fall into similar ranges as observed for standard B-DNA. Conformational deviations in the backbone can be partly attributed to the chemical changes in the nucleosides, generating bicyclic sugar moieties (bcDNA). From this short fragment, an extended parallel-stranded duplex was generated and its helical parameters were analyzed.

Introduction

Selective inhibition of protein biosynthesis, as pursued by the antisense strategy (1), depends to a great extent on the derivation of oligonucleotide analogues with stronger binding to complementary DNA and RNA molecules relative to native oligonucleotides. In addition, analogues should be more resistant to nucleases compared to their natural counterparts, but maintain their capability of permeating membranes. Possible sites for chemical alterations with nucleic acids include changes at the internucleotide phosphate bridge and at the sugar, as well as at the base portions of the nucleoside units (2). Modifications of the phosphate group comprise the non-bridging phosphate oxygens [e.g. methylphosphonates (3) and phosphorothioates (4)] and the bridging phosphate oxygens (5), as well as the replacement of the entire phosphate group in dephospho-internucleotide analogues. Other analogues feature nucleotides with α-anomeric deoxyriboses as the sugar building blocks (6). Recently, peptide-like structural elements and nucleic acid bases were combined to so-called peptide nucleic acids (PNAs; (7)).

Pairing stability can be enhanced through the influence of either enthalpy or entropy. Evolutionary aspects of nucleic acid structure formed the background for an investigation of the pairing properties of oligo-2′,3′-dideoxyglucopyrano-nucleotides

* Author to whom correspondence should be addressed.

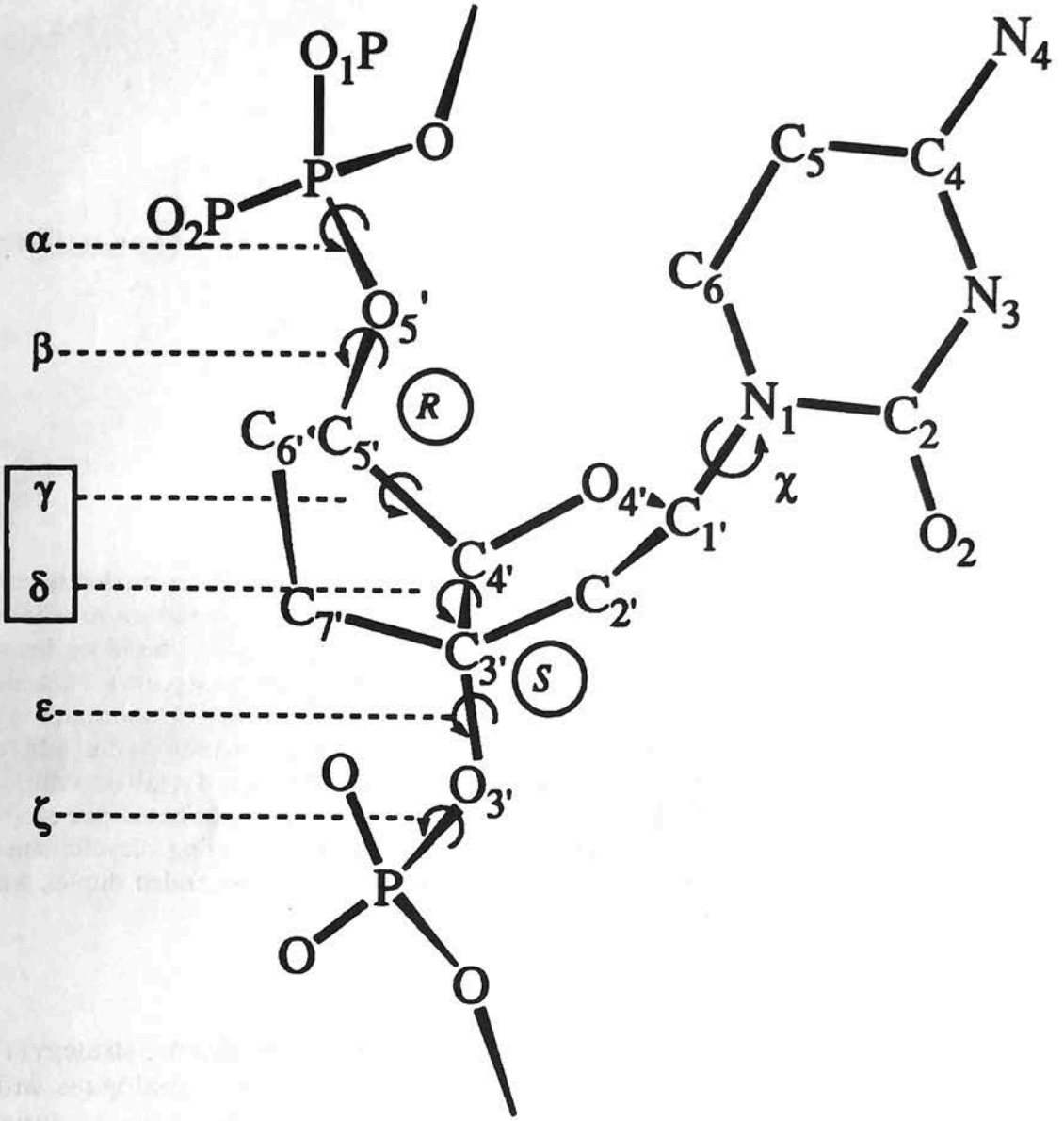

Figure 1: Configuration and conformation of a bicyclo (bc) -DNA single strand. The carbon atoms of the ethylene bridge generating the bicyclic furanose moiety are numbered C(6′) and C(7′). The six torsion angles α to ζ characterizing the conformation of the repeated nucleotide unit, as well as the glycosyl torsion angle χ are labeled. Torsion angles with limited rotational freedom as a consequence of the chemical modification of the sugar are highlighted. Atoms are numbered and the absolute configurations at carbons C(3′) and C(5′) are shown in italics.

(homo-DNA; (8,9); and references cited therein). These studies have demonstrated that homo-DNA duplexes with purine-pyrimidine base pairing are thermodynamically more stable than the corresponding DNA duplexes. This stability difference is not enthalpic but purely entropic in origin, and seems to be a consequence of the higher conformational preorganization of the homo-DNA single strand toward duplexation. The concept of entropically stabilized duplexation has stimulated the exploration of structurally altered DNAs with a higher degree of pairing preorganization compared to native DNA, and possibly increased stability of mixed complexes between the DNA analogue and DNA or RNA strands.

In so-called bicyclo-DNA (bcDNA), intranucleosidyl ethylene bridges between

deoxyribose carbon atoms C(3′) and C(5′) were introduced synthetically in order to restrict the conformational freedom of the DNA backbone (Figure 1; (10)). The configuration of the resulting chiral center at carbon C(5′) is *R*, whereas the configuration at C(3′) remains *S*. Of the six torsion angles characterizing the DNA backbone conformation, one can expect torsions γ and δ to be largely restricted in their rotational freedom for bcDNA compared to native DNA (Figure 1). X-ray and NMR experiments with bcDNA nucleosides displayed the preference for an *S*-type sugar pucker, whereas the C(3′)-*endo* conformation is disfavored due to steric interactions between the ethylene bridge and the base substituent (10). The incorporation of an ethylene bridge between the two furanose carbons generates a tertiary phosphodiester group, which should lead to an altered resistance of bcDNA against enzymatic degradation compared to native DNA. The results of UV-melting and -mixing experiments with complexes containing bcDNA strands can be summarized as follows (11,12): (1) The complex between $bc(A)_{10}$ and poly(U) is considerably more stable than the native DNA-RNA hybrid. (2) Contrary to the native $d(A)_{10} \cdot [d(T_{10})]_2$ system, triplexes of this type, containing at least one bicyclic strand, can form under nearly physiological conditions. (3) Duplexes containing at least one bicyclic strand are stabilized entropically, whereas ΔH is slighly reduced relative to native duplexes. (4) $bcd(T)_{10}$ is more resistant to degradation by various nucleases compared to the corresponding DNA.

Here we report the X-ray crystal structure of the bicyclic analogue of the DNA dinucleotide deoxycytidylyl-(3′-5′)-deoxycytidine. This first high-resolution crystal structure of a double-stranded homo-pyrimidine fragment provides some evidence for the double helical nature of poly(dC). A brief description of the $[bcd(C)_2]_2$ duplex has been published elsewhere (13). In this contribution, we provide more details of the conformation and lattice interactions of the parallel-stranded duplex, and describe the extension of the dinucleotide unit to a longer parallel-stranded $[bcd(C_8)]_2$ duplex.

Materials and Methods

Synthesis and Purification

Synthesis of the nucleoside monomers from a common bicyclic sugar compound and the corresponding bases was described previously (10). The $bcd(C_2)$ dinucleotide (172μmole) was prepared by standard phosphoramidite chemistry in solution with suitably protected monomers (14). Purification of the crude deprotected dimer was performed by column chromatography (silica gel, iprOH:conc. NH_3=3:1), and yielded 86mg (88%) $bcd(C_2)$ (ammonium form). Purity of the material was checked by NMR (^1H, ^{13}C, ^{31}P) and MS.

Crystallization and Data Collection

Single crystals were grown at room temperature by the vapor diffusion technique. Sitting drops with volumes between 10 and 20μl of a solution of 12mg $bcd(C_2)$ per ml water (20mM, single strand ammonium salt) were equilibrated against a reservoir of 25ml methanol. Square-shaped crystals with typical dimensions of 0.5 × 0.5 × 0.2mm

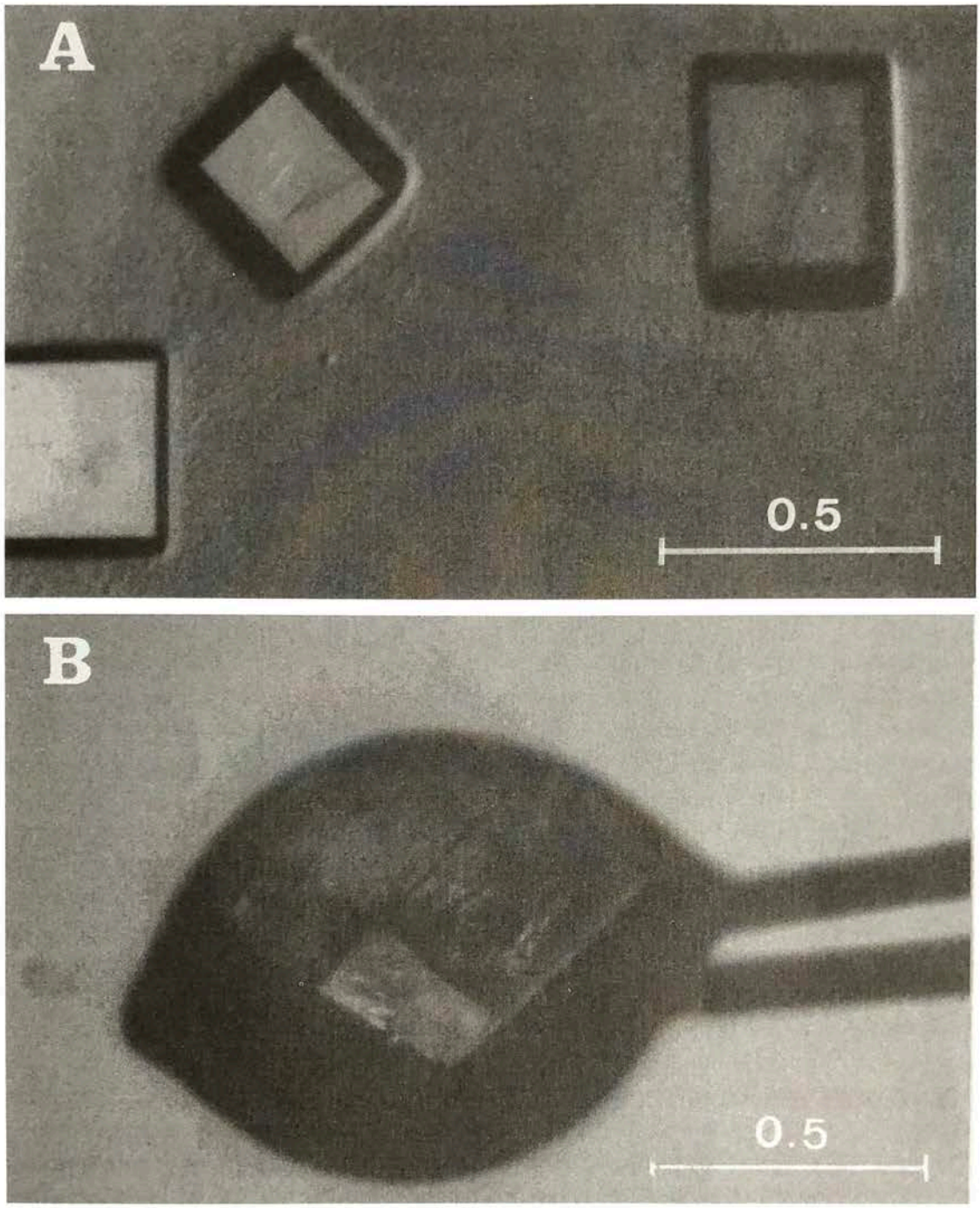

Figure 2: (A) Single crystals of bcd(C_2). **(B)** A crystal sealed in a droplet of 2-component epoxy glue at the tip of a glass fiber. White bars indicate the dimensions of the crystals in mm.

grew in the course of about a week (Figure 2A). Despite their perfect appearance the crystals turned out to be extremely fragile and difficult to handle. Sealing the crystals in a glass capillary with a droplet of mother liquor caused decay within minutes, and cooling to various temperatures between +10 °C and −130 °C (flash freezing method) did not prevent decay within a few hours. Crystals could only be mounted without cracking or turning opaque by picking them directly out of the solution with a droplet of Araldit® (CIBA-GEIGY), and sealing them in the glue (Figure 2B). Crystals then remained stable for about a week. Data were collected at 0 °C on a four-circle diffractometer (Enraf Nonius CAD4) with graphite-monochromatized

Table I
Selected Crystal and Refinement Data

Space Group	$P2_1$	Used ($I>2\sigma(I)$)	2556
a[Å]	13.37(1)	Resolution [Å]	1.04
b[Å]	19.11(4)	*R*-Factor[1]	9.3%
c[Å]	13.37(1)	Solvent	$7H_2O/4MeOH$
β[°]	91.45(7)	ρ_{exp}[g cm^{-3}][2]	1.36
Volume [Å^3]	3414(4)	ρ_{calc}[g cm^{-3}]	1.35
Z	4	Average SD for bond lengths	<0.03 Å
Unique Reflections	3304	Average SD for bond angles	<2°

[1] $1/\sigma^2$ weights.
[2] Floating method, carbon tetrachloride/o-xylene density gradient.

MoK_α radiation and processed as described previously (13). Maximum decay was checked with three independent reflections and was less than 0.6%. Crystal data, reflection statistics and selected refinement parameters are listed in Table I.

Structure Determination and Refinement

The structure was solved with the direct methods program Shelxs-86 (15), using an extended number of phase generation cycles. Fourier electron density maps revealed 47 of the totally 78 heavy atoms of the duplex. The missing atom positions were located in a difference electron density map, calculated after several rounds of least-squares refinement with the program Bigshelx-76 (16). The complete duplex was then refined with the program Shelxl-92 (17), including 2556 reflections with $I>2\sigma(I)$. Base atoms of residues C[2] and C[4] were restrained to planarity due to slight pyramidalisation of the N(1) atoms during unrestrained refinement, and distances of the C(1′)-N(1) bonds of the same residues were kept at 1.46 Å with a standard deviation of ±0.1 Å. At an *R* factor of 15%, Fourier electron sum ($2F_o$-F_c) and difference (F_o-F_c) density maps were calculated with the program package CCP4 (18). The maps were then displayed on an Evans&Sutherland ESV workstation using the program Chain (19). A total of 15 solvent atoms (7 water molecules and 4 methanol molecules) were located in the maps and included in the refinement. The calculated crystal density (ρ_{calc}) was then in good agreement with the measured density ρ_{exp} (see Table I). All atoms of the duplex, except N(4), C(4) and C(2′) of residue C[1], and atom C(1′) of residue C[2], were refined anisotropically. Isotropic displacement parameters of solvent atoms were kept at U=0.2 Å^2. Positions of hydrogen atoms of the $[bcd(C_2)]_2$ duplex, except for those of the hydroxyl groups, were calculated (C-H and N-H bond lengths restrained to 1.08 Å), and their isotropic displacement parameters were fixed. Positions of hydrogen atoms of methanol carbon atoms were calculated and included in the refinement; hydrogen atoms of water molecules were omitted in the refinement. The final asymmetric unit contained 93 heavy atoms and refinement was terminated at an *R* factor of 9.3% ($1/\sigma^2$ weights).

Results and Discussion

Overall conformation of the $[bcd(C_2)]_2$ duplex

In the crystal, a non-crystallographic pseudo twofold axis rotates one $bcd(C_2)$ single strand into another, generating a segment of a parallel right-handed double helix.

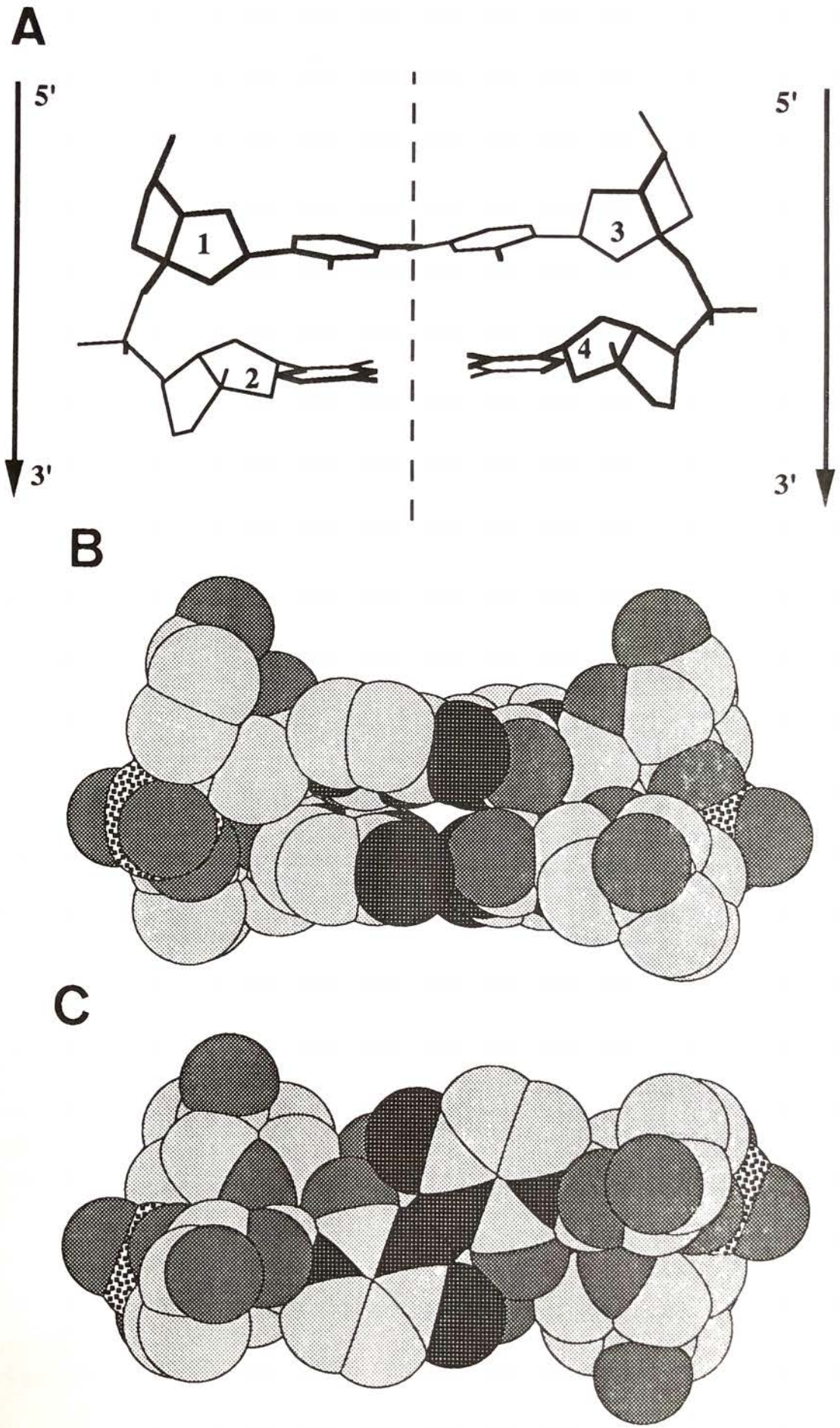
A
5'
3'
1
2
3
4
5'
3'
B
C

Figure 3: (A) Skeletal representation of the $[bcd(C_2)]_2$ duplex, viewed into one of the two identical grooves. Residues are labeled 1 to 4, and arrows indicate the parallel orientation of strands with both 5′-termini at the top. The two strands are related by a non-crystallographic pseudo twofold rotation axis, coinciding with the helix axis (dashed line). **(B)** Van der Waals model of the duplex viewed into the groove, roughly perpendicular to the non-crystallographic twofold rotation axis (helix axis). Carbon atoms are stippled in light grey, oxygen atoms are stippled in dark grey, nitrogen atoms are stippled in black, and phosphorus atoms are hatched. **(C)** Van der Waals model of the duplex viewed along the non-crystallographic twofold rotation axis, roughly perpendicular to the best plane through the base pair at the top. Atom types are coded according to Figure B.

Unlike in antiparallel duplexes, where twofold rotation axes are located in and half-way between base pair planes, the twofold axis in the parallel duplex falls nearly together with the helix axis (Figure 3A). The duplex has 10.5 residues per turn with a helical twist of 34.3° and a helical rise of 3.25 Å [calculated with program NEWHELIX (version NEWHEL90, (20))]. For the determination of the helix operator, pairs of N(1) and C(1′) atoms from each of the two single strands forming the duplex were used.

Cytosine bases are paired via three hydrogen bonds with an average hydrogen bond length of 2.83 Å (longest hydrogen bond N4 · · · O2, base pair C[2] · C[4]: 2.88 Å; shortest hydrogen bond N3 · · · N3, base pair C[2] · C[4]: 2.74 Å). Both, roll and tilt between base pairs are 0.3°, and the inclinations for base pairs C[1] · C[3] and C[2] · C[4] are 2.8 ° and 3.5°, respectively. The tip for base pair C[1] · C[3] is 2.6°, and for base pair C[2] · C[4], it is 1°. In both C-C^+ pairs, bases display considerable propeller twists. For base pair C[1] · C[3], the twist angle is 12°, and for base pair C[2] · C[4], it is −15°. The base pairs are buckled in opposite directions, but whereas the buckle for base pair C[1] · C[3] is 27°, the stacked base pair is almost planar with a buckle of only −1°. Both base pairs show only insignificant sliding, shearing, and x- and y-displacement in the parallel-stranded duplex.

The distances between C(1′) atoms for base pairs C[1] · C[3] and C[2] · C[4] are 9.62 Å and 9.55 Å, respectively. These values are only about 1 Å shorter than the corresponding distances in antiparallel duplexes with Watson-Crick type purine pyrimidine base pairs (21,22). The *anti* Watson-Crick arrangement of cytosines in the C-C^+ base pairs observed here, with both glycosyl torsions lying in the anti range, results in a *trans* position of glycosyl bonds (23). Therefore, C(1′) atoms lie on opposite sides relative to the helix axis, resulting in distances between them which are similar to the ones found between C(1′) atoms of purine-pyrimidine base pairs in A- and B-type duplexes. Similarly, the distance of 17 Å between interstrand phosphorus atoms in the $[bcd(C_2)]_2$ duplex is not too different from the one observed for antiparallel double helices (ca. 17.5 Å). Despite such similarities in the overall dimensions of antiparallel duplexes and the parallel duplex described here, their topologies are entirely different. In the $[bcd(C_2)]_2$ duplex, the arrangement of cytosines in C-C^+ base pairs with three hydrogen bonds creates two identical grooves with the same functional groups, related by a twofold rotation (Figure 3C). The groove width in the parallel duplex is comparable to the major groove width in B-DNA, whereas the depth lies in between those of the B-DNA major and minor grooves.

Another consequence of the superpositioned helix and twofold rotation axes is the arrangement of corresponding nucleotide atoms from the two strands at identical

heights with respect to the helix axis, rather than shifted along the helical axis in opposite directions, as in antiparallel duplexes. Two conformationally similar strands (e.g. two DNA strands, but not necessarily a DNA and an RNA strand) with inclined backbone to base axes cannot form parallel duplexes. An orthogonal relative orientation of backbone and base axes in the strands therefore is a prerequisite for the formation of a parallel double helix, such as the one described here [see (9) for a somewhat related treatment of geometrical aspects of pairing between {idealized} linear oligonucleotide strands with antiparallel strand orientation]. Thus, in parallel-stranded double helices of the type described here, one would expect only minimal base roll, tilt, sliding and displacements. This is consistent with the observed values for these parameters in the case of the $[bcd(C_2)]_2$ duplex.

Base Stacking and Pairing Mode

The values of 34° for helix twist and 3.25 Å for rise are somewhat reminiscent of those observed for helices with B-type geometry. The B-like parameters result in strong stacking interactions between adjacent C-C^+ base pairs in the $[bcd(C_2)]_2$ duplex (Figures 3 B,C). The midpoints between hydrogen-bonded N(3) atoms for both base pairs are located on the non-crystallographic twofold rotation axis relating the two strands. Since there is no offset between stacked base pairs, there is considerable overlap between cytosine bases from adjacent pairs. Thus, the C(2) atom of one cytosine base is positioned above the center of the six-membered ring from the stacked base, and the latter one has its C(4) atom positioned roughly above the center of the ring from the first cytosine base in turn. This arrangement leads to a positioning of the C(2)=O(2) carbonyl groups from stacked cytosine bases, such that the keto oxygen of one cytosine is located more or less above the keto carbon from the stacked base (Figure 3C). The two base pairs in the $[bcd(C_2)]_2$ duplex are propeller-twisted in opposite directions (Figure 3B), resulting in close contacts between pairs of C(2) and O(2) atoms from stacked bases (2.88 and 2.91 Å, resp.). This is an indication that the two resulting dipole-dipole interactions per base pair contribute significantly to the stability of the $[bcd(C_2)]_2$ duplex.

In principle, it is possible to determine the protonation state of a cytosine base from its precise geometry (24,25). For a protonated cytosine base, the angle C(2)-N(3)-C(4) is widened up, whereas the expected value for a neutral base is close to 120°. The adjacent bond angles N(1)-C(2)-N(3) and N(3)-C(4)-C(5) in the ring are usually smaller in the protonated form. Another angle which was found to be very sensitive to protonation is N(1)-C(2)-O(2). The angles at atom N(3) for residues 1 to 4 are 124.1(1.7)°, 120.4(2.1)°, 121.2(1.8)° and 119.9(2.1)°, respectively (standard deviations in parentheses). For angle N(1)-C(2)-O(2), the values are 121.6(2.3)°, 117.94(2.0)°, 124.1(2.2)° and 120.4(2.1)° for the four residues, respectively. These angle pairs can then be used to discriminate between the protonated and unprotonated forms with the help of an empirical formula (24). In the case of the two base pairs in the $[bcd(C_2)]_2$ duplex, the values obtained from this discriminant function indicate that the cytosine bases of residues 1 and 3 are protonated, and that those of residues 2 and 4 are in the neutral form. A simultaneous protonation of bases in the C[1] · C[3] pair is obviously impossible. Similarly, the observed pairing mode requires the presence of one proton

per base pair, which renders the indicated neutral state for base pair C[2] · C[4] irrelevant. However, statements with high probabilities regarding the protonation state require precisely determined bond lengths and angles. In the present structure, the estimated standard deviations for bond lengths are 0.03 Å, and for bond angles, they are 2°. An unambiguous discrimination between protonated and unprotonated state using the above rules may therefore not be possible. In addition, bond lengths and planarity restraints were used for some of the residues during refinement, and the resulting values for bond lengths and angles may be the reason for the irrelevance of the numbers obtained from the discriminant function.

Backbone and Sugar Conformation

The backbone conformation of oligonucleotides is usually characterized with six torsion angles α to ζ for each of the nucleotide units (Figure 1). The conformational flexibility of the furanose ring with accompanying changes of torsion angle δ[C(5′)-C(4′)-C(3′)-O(3′)] is the underlying cause of the dramatic topological differences between the A-DNA and B-DNA conformers. In B-DNA, δ is in the *ap* range, and distances between adjacent intra-strand phosphorus atoms range from 6.5 to 7.0 Å. Changing δ to the +*sc* conformation, as found in A-type double helices, results in a reduction of the distance between adjacent phosphorus atoms to about 5.5 Å. From Figure 1, it is apparent that in the bicyclic oligonucleotide, the torsion angles most likely to be restricted in their rotational ranges are angles γ and δ. X-ray experiments, NMR solution studies, as well as molecular modeling with mononucleosides are consistent with a less flexible furanose conformation in bcDNA, and the preference of an S-type sugar pucker (10). In the crystal structure of the bcd(T) nucleoside, the furanose adopts a C(1′)-*exo* conformation (δ = 127°). This structure, as well as proton NMR spectra with other nucleosides in solution, supported the preference of an *anti* conformation of the glycosyl torsion angle χ at least with bicyclic pyrimidine nucleosides.

The crystal structure of bcd(C_2) confirms the expectations based on earlier studies, showing a preference for S-type pucker by the furanose in the bycyclic sugar framework. In the case of residues 1 and 3, the furanose rings adopt C(1′)-*exo* conformation. The furanoses of residues 2 and 4 adopt C2′-*endo* conformation. Thus, the two sugar moieties of the bcd(C_2) single strands constituting the duplex have different puckers. The sugar puckers of base-paired residues are very similar, as indicated by the only small differences between individual ring torsion angles (Table II). C(1′)-*exo* and C(2′)-*endo* conformation are direct neighbors in the pseudorotation phase cycle. Both are found for the deoxyriboses in B-DNA duplexes, and in the dodecamer with the sequence d(CGCGAATTCGCG), the C(1′)-*exo* conformation is found in 11 of the 24 nucleotides, whereas the C(2′)-*endo* conformation occurs 9 times. Thus, the additional ethylene bridge linking atoms C(5′) and C(3′) in bcDNA appears not to alter the furanose conformation found in B-type duplexes in a dramatic way.

The backbone torsion angles for both bcd(C_2) strands fall into the ranges −*sc*, *ac*, *ac*,

Table II

Pseudorotation parameters and glycosyl torsion angles for the $[bcd(C_2)]_2$ duplex. Torsion angles in degrees for all four residues are listed for the furanose ring, as well as for the carbocyclic ring. P is the pseudorotation phase angle, and P^*, the pseudorotation phase angle for the ring constituted by atoms C(3′), C(4′), C(5′), C(6′) and C(7′), is defined below. Torsion angles in the two five-membered rings are defined in the two drawings.

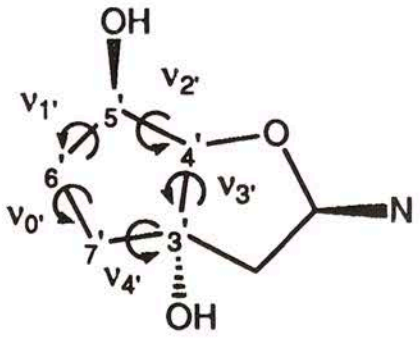

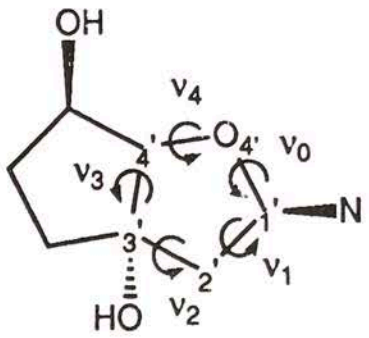

					Res 1	Res 2	Res 3	Res 4
C4'	O4'	C1'	C2'	ν_0	-38	-8	-40	-9
O4'	C1'	C2'	C3'	ν_1	32	16	34	16
C1'	C2'	C3'	C4'	ν_2	-15	-16	-16	-16
C2'	C3'	C4'	O4'	ν_3	-7	12	-5	11
C3'	C4'	O4'	C1'	ν_4	27	-3	29	-2
				P	114	170	115	166
C3'	C7'	C6'	C5'	$\nu_{0'}$	49	44	39	43
C7'	C6'	C5'	C4'	$\nu_{1'}$	-51	-36	-44	-37
C6'	C5'	C4'	C3'	$\nu_{2'}$	35	16	32	18
C5'	C4'	C3'	C7'	$\nu_{3'}$	-4	12	-5	10
C4'	C3'	C7'	C6'	$\nu_{4'}$	-26	-35	-19	-34
				P^*	-49	-69	-45	-66
O4'	C1'	N1	C2	χ	-107	-143	-108	-146

$$\tan P^* = \frac{(\nu_{4'} + \nu_{1'}) - (\nu_{3'} + \nu_{0'})}{2 * \nu_{2'} * (\sin 36^\circ + \sin 72^\circ)}$$

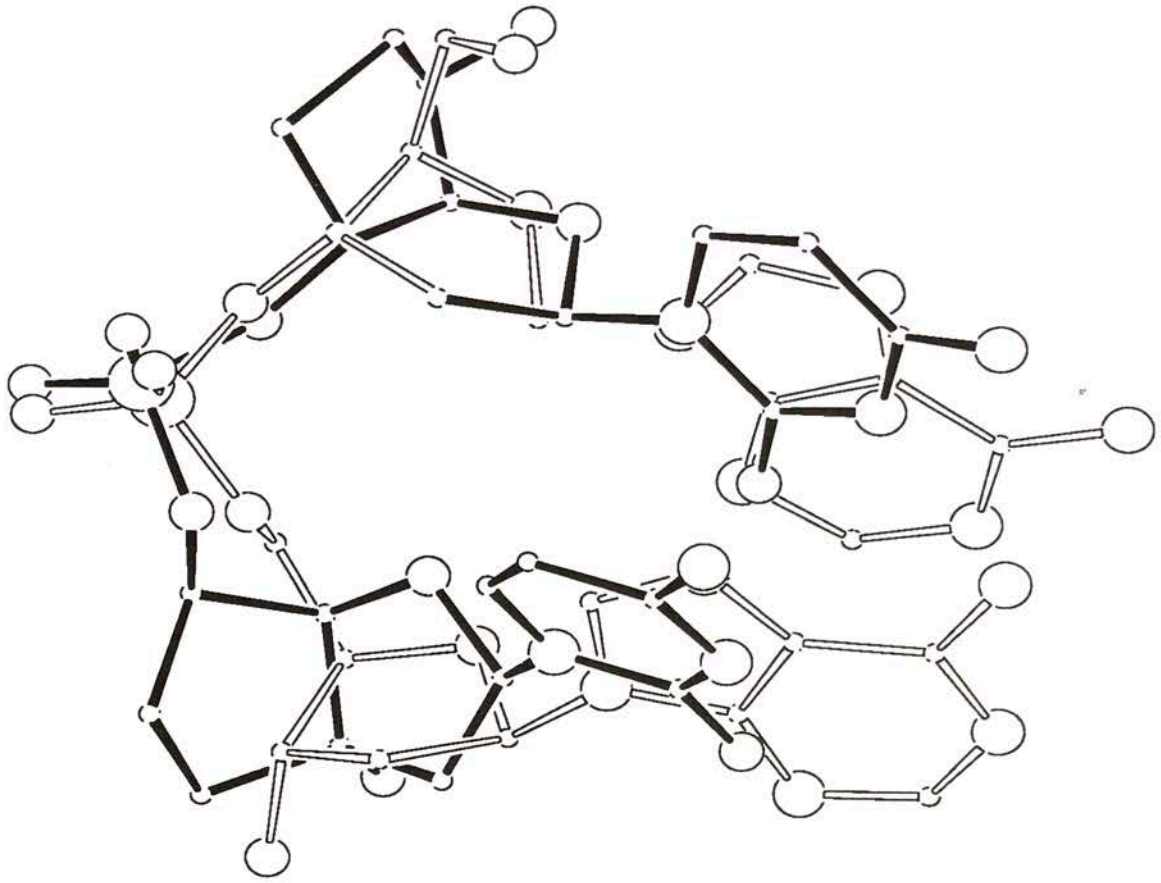

Figure 4: Superposition of the crystal structures of one of the bcd(C_2) strands (residues C[1] and C[2], solid bonds) and the d(A[5]A[6]) dinucleotide (open bonds) from the B-DNA dodecamer d(CGCGAATTCGCG) (26). Only backbone and sugar atoms [omitting carbon atoms C(6′) and C(7′) of the bcDNA dimer] were used for the superposition (27). The rms deviation between the dimers is 0.4 Å with a maximum deviation of 1.4 Å between atoms C(5′) of residues C[2] and A[6]. Atom types are coded according to size with P>N>O>C.

residues 1 and 2 is 18° (154 vs. 136°), and for the δ angles, the difference is 24° (111 vs. 135°). The difference between the γ angles of residues 3 and 4 is 26° (159 vs. 133°), and for the δ angles, the difference is 17° (115 vs. 132°). Compared to a B-DNA backbone, torsion angles β are smaller and torsion angles γ are larger in the [bcd(C_2)]$_2$ duplex. These conformational alterations result in relative shifts between the O(5′) atoms of the B-DNA and bcDNA backbones (Figure 4). However, the positionings of the furanoses are not altered much as a consequence of such changes in the backbone. Rather, the positions of atom pairs C(4′) and C(1′) in the B-DNA and bcDNA backbones are only differing slightly. The most obvious change is the rotation of the furanose rings of residues C[2] and A[5] relative to each other, resulting in a considerable shift between O(3′) atoms (see bottom Figure 4). The deviations between the two dimers are partially caused by the fact, that in the bcd(C_2) dimer, the two sugar puckers are different, whereas the furanoses of residues A[5] and A[6] both adopt C(1′)-*exo* puckers. In particular, the seemingly large deviations between the positions of N(1) atoms in bcd(C_2) and those of N(9) atoms in d(A_2) are partially due to the different sugar puckers in the compared dimers. The glycosyl torsion angles for all four residues in the [bcd(C_2)]$_2$ duplex fall into the *anti* range (Table II). However, the average values for base-paired residues differ by 38° for base pairs C[1] · C[3] and C[2] · C[4].

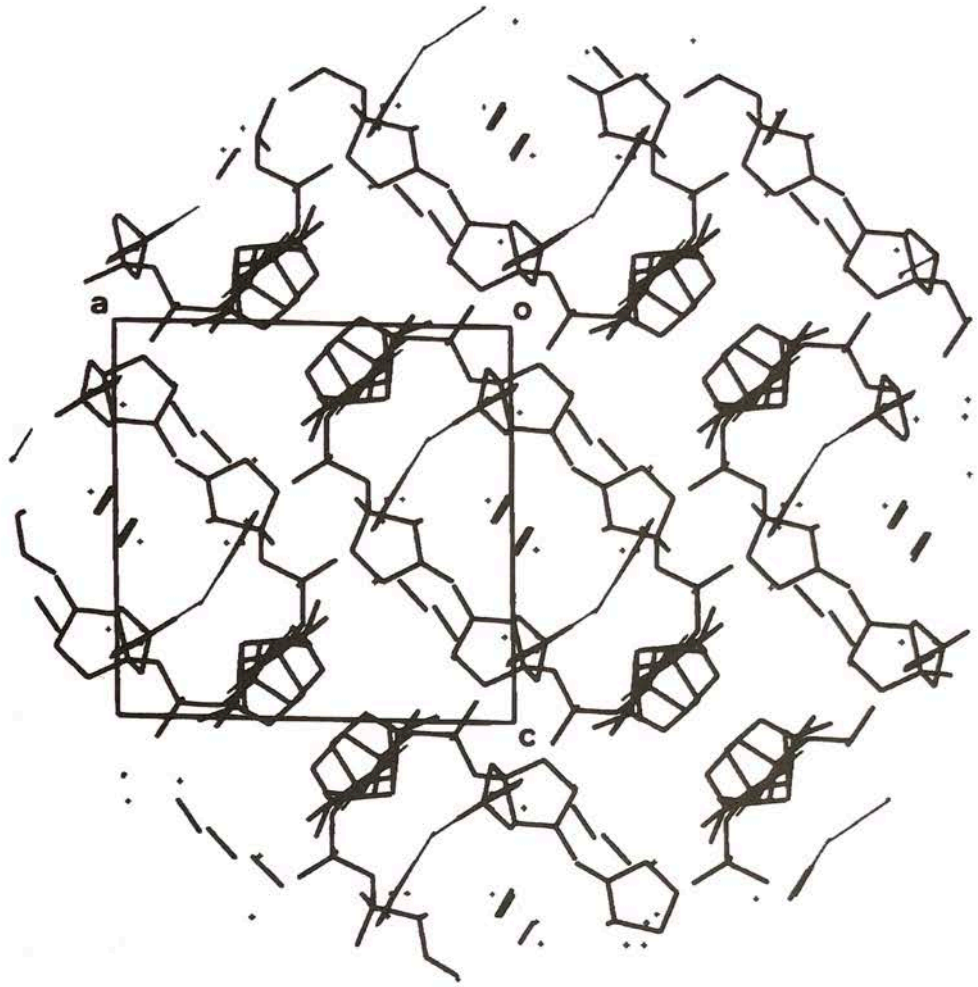

Figure 5: Packing arrangement in the bcd(C_2) crystal lattice viewed along the monoclinic *b*-axis. The drawing shows a sphere of 15 Å radius, centered around atom C(11) of a methanol molecule. The unit cell is outlined, crosses are water molecules, and dashes are methanol molecules.

Similar to the pseudorotation phase angle for the furanose ring, one can define a corresponding parameter to describe the conformation adopted by the carbocyclic five-membered ring in bcDNA nucleotides (Table II). The torsion angles in these rings vary to a smaller degree compared to the furanose rings. As a result, the pseudorotation phase angles *P** differ only by about 20° between intrastrand residues C[1] and C[2], and between C[3] and C[4].

Lattice Interactions and Hydration

The *a* and *c* cell constants of bcd(C_2) crystals are very similar and the monoclinic β angle is close to 90° (Table I). In addition to the unit cell dimensions, there are other features of the crystal packing in the bcd(C_2) structure which are reminiscent of tetragonal space groups. Two families of non-crystallographic twofold rotation axes run diagonally to the *x*- and *z*-directions, almost perpendicular to each other. The non-crystallographic twofolds are located at different heights with respect to the monoclinic *y*-axis. The nearly perfect twofold rotation axes running along the [10-1] direction and through the midpoints of the *a* and *c* axes are intramolecular, and relate single bcd(C_2) strands to one another (Figure 5). The high degree of pseudo

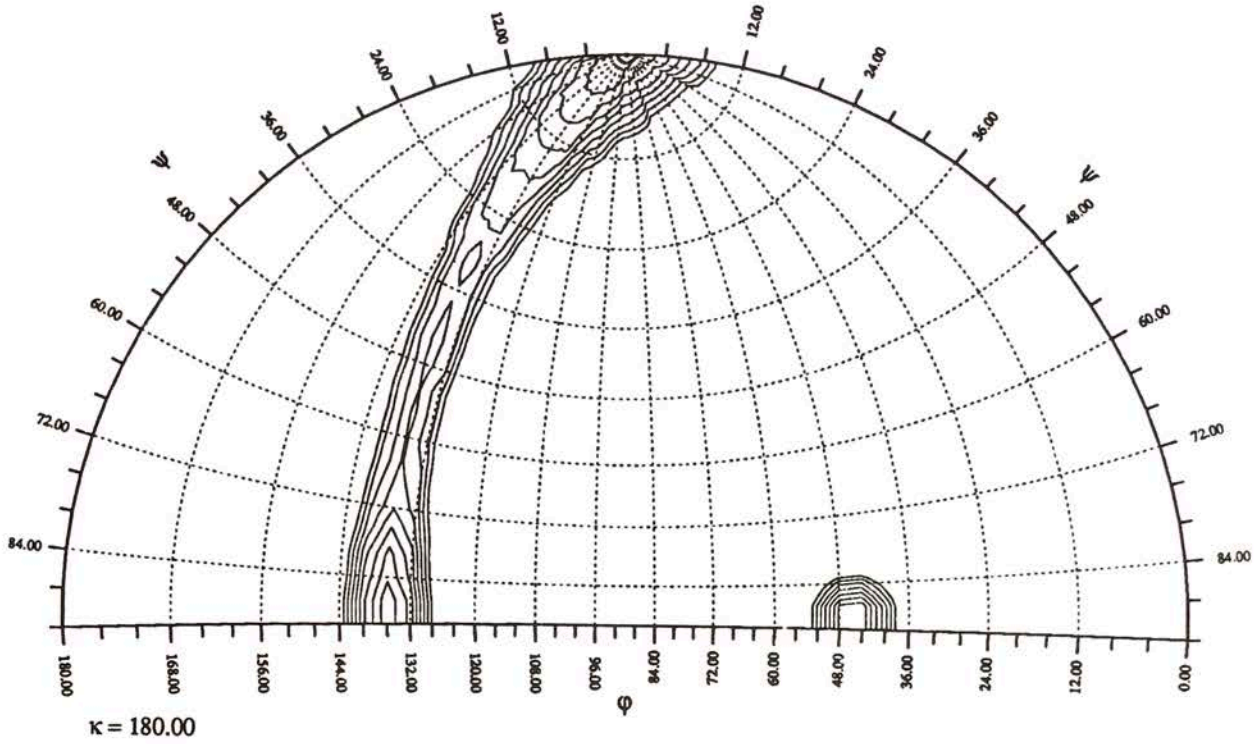

Figure 6: Self-rotation function for bcd(C_2). The plot was generated with program GLRF [version 1.1, (28)], using data with $F>1\sigma(F)$ between 15 and 1 Å, with a 5 Å radius of integration. The axial peak at $\psi=0°$ and $\varphi=0°$ is produced by the crystallographic twofold screw axes running along the *y*-direction in space group $P2_1$. The two peaks at $\psi=90°$ and $\varphi=45°$ (intramolecular, see text) and $\psi=90°$ and $\varphi=135°$ (intermolecular) indicate the presence of non-crystallographic twofold rotation axes perpendicular to the unique axis, and approximately perpendicular to one another. The definition for polar angles ϕ, ψ and κ is given in (29).

symmetry is indicated by the small rms deviation between the two bcd(C_2) single strands generating the duplex (0.02 Å). In addition, the self-rotation function reveals two local twofold axes, one of which gives rise to quite a sharp peak, corresponding to the above intramolecular axes (Figure 6). The more approximate non-crystallographic twofolds running along the [101] direction are intermolecular, and relate $[bcd(C_2)]_2$ duplexes to one another (Figure 5). The extended appearance of the corresponding peak in the self-rotation function indicates a set of pseudo twofold axes lying in the (10-1) plane (Figure 6).

From Figure 5, it can be seen that the cytosine base planes of duplexes are arranged diagonally, approximately along the [101] direction. There are no intermolecular stacking interactions between the cytosine bases in the bcd(C_2) crystal. This may account for the extreme fragility of the crystals. Within the infinite stacks of duplexes, generated by the twofold screw axes running along the crystallographic *y*-direction, bases are oriented with their edges facing each other (Figure 5). Within *xy*-layers, duplexes face each other with their 5′-termini and with their 3′-termini in an alternating manner (Figure 5). The offset in *y* between adjacent duplexes prevents intermolecular base stacking, and leads to direct or solvent-mediated hydrogen bonding

Table III

Hydrogen bonding interactions of the two bcd(C_2) strands in the crystal. The table lists the hydrogen bonding partner and its residue (in brackets), as well as the rotational (in italics, *1* = [*x,y,z*] and *2* = [*−x,y+1/2,−z*]) and translational components (in parentheses) of the symmetry operator (from left to right). O1W to O7W are water molecules, and O8 to O11 are oxygen atoms of methanol molecules. Base-base hydrogen bonds are boxed and distances (bold) are in Å.

	Residue 1	Residue 2	Residue 3	Residue 4
O3′		O1P[4]*1*(0-1 0) **2.77**		O1P[2]*1*(0 1 0) **2.76**
O4′	O5′[3]*2*(0-1 1) **2.87**		O5′[1]*2*(0 0 1) **2.94**	
O5′	O4′[3]*2*(0-1 1) **2.94**		O4′[1]*2*(0 0 1) **2.87**	
	O5′[3]*2*(0-1 1) **2.87**		O5′[1]*2*(0 0 1) **2.87**	
	O8 *2*(0-1 1) **2.71**		O11 *2*(0 0 1) **2.87**	
O2	N4[3]*1*(0 0 0) **2.86**	N4[4]*1*(0 0 0) **2.83**		
N3	N3[3]*1*(0 0 0) **2.83**	N3[4]*1*(0 0 0) **2.74**		
N4	O2[3]*1*(0 0 0) **2.86**	O2[4]*1*(0 0 0) **2.88**		
	O2P[2]*2*(1 0 1) **2.83**	O1Ø *1*(0 0 0) **2.78**	O2P[4]*2*(0-1 0) **2.81**	O9 *1*(0 0-1) **2.76**
O1P		O3′[4]*1*(0-1 0) **2.76**		O3W*1*(0 0 0) **2.87**
		O4W*1*(0-1 0) **2.96**		O3′[2]*1*(0 1 0) **2.77**
O2P		N4[1]*2*(1-1 1) **2.83**		N4[3]*2*(0 0 0) **2.81**
		O2W*2*(1-1 1) **2.69**		O1W*1*(0 0-1) **2.86**

Table IV

Hydrogen bonding interactions of solvent molecules in the bcd(C_2) crystal. Identical conventions as in Table III were used, and distances (bold) are in Å.

O1W	O7W	*1*	(0 0 0)	**2.48**
	O2P[4]	*1*	(0 0 1)	**2.86**
O2W	O6W	*1*	(0 0 0)	**2.23**
	O2P[2]	*2*	(1 0 1)	**2.69**
O3W	O1P[4]	*1*	(0 0 0)	**2.87**
	O5W	*2*	(1 0 1)	**3.09**
	O7W	*2*	(0 0 1)	**2.83**
	O9	*2*	(0 0 1)	**2.78**
O4W	O1P[2]	*1*	(0 1 0)	**2.96**
	O5W	*2*	(1 0 1)	**2.99**
	O1Ø	*2*	(1 0 1)	**2.73**
O5W	O3W	*2*	(1-1 1)	**3.09**
	O4W	*2*	(1-1 1)	**2.99**
	O8	*1*	(1 0 0)	**2.81**
	O11	*1*	(1 0 0)	**2.57**
O6W	O2W	*1*	(0 0 0)	**2.23**
O7W	O1W	*1*	(0 0 0)	**2.48**
	O9	*1*	(0 0 0)	**3.06**
	O3W	*2*	(0 0 0)	**2.83**
O8	O5′[1]	*2*	(0 0 1)	**2.71**
	O5W	*1*	(-1 0 0)	**2.81**
O9	O7W	*1*	(0 0 0)	**3.06**
	N4[4]	*1*	(0 0 1)	**2.76**
	O3W	*2*	(0-1 1)	**2.78**
O10	N4[2]	*1*	(0 0 0)	**2.78**
	O4W	*2*	(1-1 1)	**2.73**
O11	O5W	*1*	(-1 0 0)	**2.57**
	O5′[3]	*2*	(0-1 1)	**2.87**

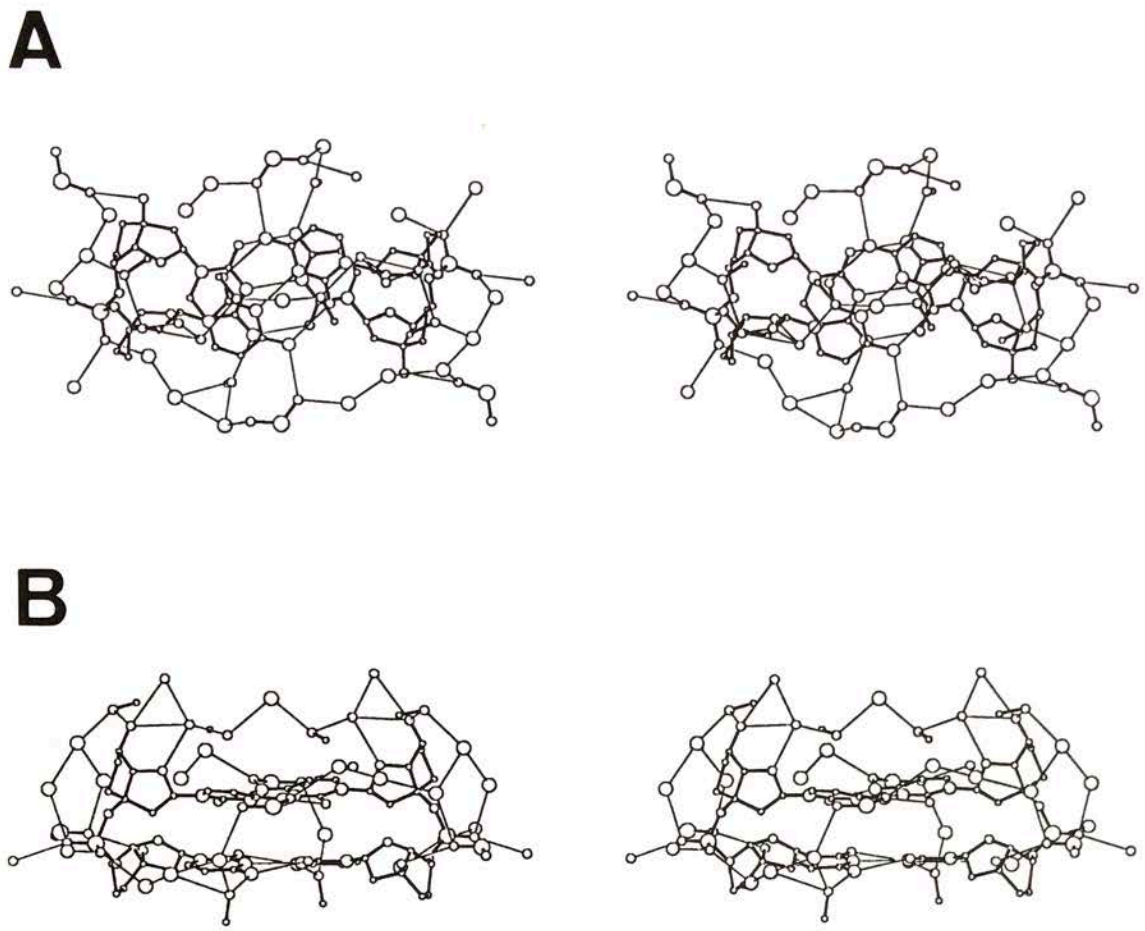

Figure 7: Stereo diagram of lattice contacts and solvent interactions of the $[bcd(C_2)]_2$ duplex, viewed (A) along, and (B) rotated by about 90°, perpendicular to the helical axis. The duplex has been oriented in a way that residue C[1] is located at the top right in Figure (B). The duplex is drawn with thick solid bonds, and atom types are coded according to size with P>N>O>C. Water molecules are drawn with largest spheres, and hydrogen bonds are thin lines.

between duplexes instead. This packing arrangement generates solvent channels bordered by either the 5′-terminal base pairs and sugar frameworks of two adjacent duplexes, or in an alternating way, by the 3′-terminal base pairs and sugar frameworks of two duplexes. Whereas there are direct hydrogen bonds between duplexes facing each other with their 5′-termini, the terminal 3′-hydroxyl groups are engaged in hydrogen bonds to phosphate groups of neighboring duplexes within stacks.

Hydrogen bonding interactions of the $[bcd(C_2)]_2$ duplex are listed in Table III, and hydrogen bonding interactions of solvent molecules are listed in Table IV. Figure 7 illustrates lattice contacts and solvent interactions of the $[bcd(C_2)]_2$ duplex. Both N(4) nitrogens from base pair C[1] · C[3] are engaged in hydrogen bonds to phosphate oxygens of residues from adjacent stacks (Figure 7A). This interaction mode is somewhat similar to the observed hydrogen bonds between these nitrogens and phosphates from neighboring duplexes in the crystal structures of $[d(CG)]_2$ with either NH_4^+ (30) or Na^+ (25) as the counterions. In the former structure, the N(4) atoms of both paired cytosine bases are hydrogen bonded to phosphate groups, whereas in the latter structure, only the contact between one phosphate group and N(4) from the cytosine base, which was found to be protonated, was interpreted as a

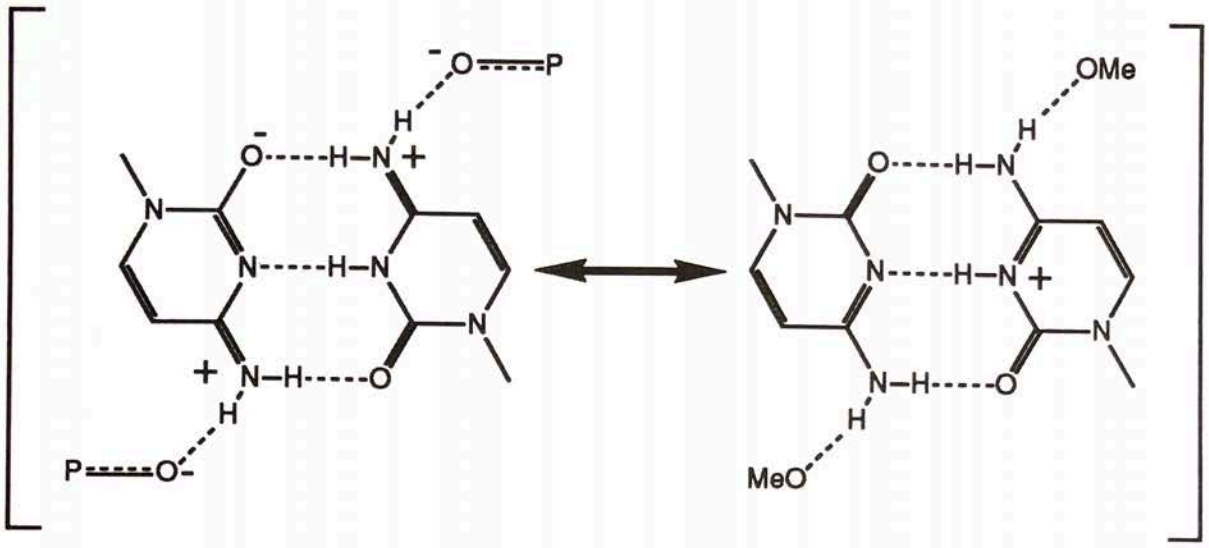

Figure 8: Possible resonance forms for a C-C$^+$ base pair. In the bcd(C_2) crystal, N(4) positions of cytosines in base pair C[1] · C[3] form hydrogen bonds to phosphates (left). N(4) positions of cytosines in base pair C[2] · C[4] form hydrogen bonds to methanol molecules (right). These different environments may indicate the presence of both resonance forms in the [bcd(C_2)]$_2$ duplex.

hydrogen bond. In the present structure, both hydrogen bonds of N(4) atoms of residues 1 and 3 are considerably shorter than the ones in the [d(CG)]$_2$ structures (2.81 Å and 2.83 Å vs. 2.9 Å and 3.17 Å, respectively, see Table III). It was mentioned before that the accuracy of the bond lengths and bond angles in the present case does not allow definitive statements as to which of the two cytosine bases per pair is protonated. The finding that the lattice contacts of the N(4) atoms of base pair C[1] · C[3] are almost identical does not shed any light on the base protonation state either. One can imagine a resonance form for a C-C$^+$ base pair, where both N(4) atoms carry positive charges and the O(2) atom of the neutral base is negatively charged (Figure 8). Such a resonance form would render the observed hydrogen bonds between N(4) atoms and negatively charged neighboring functions favorable. However, neither of the O(2) oxygens in the above base pair forms any hydrogen bonds. Interestingly, both N(4) atoms of base pair C[2] · C[4] are hydrogen bonded to methanol molecules (Figure 7 A,B). As in the case of the first base pair, none of the O(2) oxygens is engaged in hydrogen bonding. Thus, it appears that in base pair C[1] · C[3], the resonance form with positively charged N(4) nitrogens seems to prevail, whereas in base pair C[2] · C[4], the positive charge seems to be located mostly on the N(3) atoms (Figure 8).

The non-crystallographic twofold rotation axis relating single bcd(C_2) strands in the duplex extends to the solvent region surrounding duplexes (Figure 7 A,B). Both terminal O(5′) oxygens in the duplex are hydrogen bonded to O(5′) and O(4′) oxygen pairs from two neighboring duplexes, as well as to a methanol molecule. These terminal O(5′) oxygens from two different neighboring strands are linked by a string of solvent molecules (Figure 7B, top). The O(5′) hydrogen bonded to O(5′) of residue C[1] is 2.87 Å from methanol O11. The O(5′) hydrogen bonded to O(5′) of residue C[3] is 2.71 Å from methanol O8. Methanol molecules O8 and O11 are then bridged by water molecule O5W (distances 2.81 Å and 2.57 Å, respectively, see Table IV). In addition, O5W is hydrogen bonded to water molecules O3W and O4W (distances

Table V

Analysis of helicities for $[bcd(C_2)]_2$ and the dinucleotide duplexes $[d(CG)]_2$ (25), and $[r(AU)]_2$ (21,32) with program GENHEL (31). Equivalent sets of atoms (probe) used to define the helix operator were: C(1′) and N(1) [probe 1]; C(1′), N(1), O(4′), and C(2′) [probe 2]; and C(1′), N(1), O(4′), C(2′), C(3′), and C(4′) [probe 3]. Helix sigma corresponds to the average deviation between crystal coordinates of probe atoms, and the coordinates of these atoms, generated by applying the helical operator . Columns rms, mean, and max list the deviations, which result from the superposition of the two dimeric single strands, generating each of the three listed duplexes, as well as the average deviations, which result from superpositions of base pairs.

	Probe	Helix Sigma[Å]	Rise [Å]	Twist [°]	rms [Å^2]	mean dev [Å]	max dev [Å]
$[bcd(C_2)]_2$	1	0.36	3.25	34.3	0.02*	0.04	C(1′)0.11
	2	1.20	3.39	34.9	0.16†	0.24	O(5′)0.54
	3	1.32	3.52	34.7	0.41‡	0.66	O(2)1.63
$[d(CG)]_2$	1	1.43	4.96	18.5	0.12	0.21	O(1P)0.52
	2	1.51	4.71	25.7	0.05	0.15	O(5′)0.24
	3	1.73	4.45	31.3			
$[r(AU)]_2$	1	0.09	2.39	28.5	0.06	0.10	O(5′)0.24
	2	0.08	2.35	29.0	0.07	0.08	N(1)0.21
	3	0.19	2.36	30.3			

* Values for the superposition of the two single strands.
† Values for the superposition of the two base pairs [without the bases, but with N(1) or N(9)].
‡ Values for the superposition of the two base pairs (all atoms).

3.09 Å and 2.99 Å, respectively). Thus, it lies at the branching point of two solvent mediated bridges between terminal 5′-hydroxyl groups and O(1P) phosphate oxygens from adjacent residues, as well as from symmetry related strands within adjacent stacks (Figure 7 A,B, extreme left and right; Tables III and IV). Across the groove (Figure 7A, bottom; Figure 7B, foreground), three water molecules link O(2P) of residue C[4] to O(1P) of a symmetry-related phosphate group, which is hydrogen bonded to N(4) of residue C[3]. Three further water molecules then link O(2P) of the latter phosphate group to a third phosphate group, which itself contacts the terminal 3′-hydroxyl group of residue C[2] from the opposite backbone. Thus, this chain of six water molecules and two neighboring phosphate groups spans the entire groove from a phosphate group of one strand to a terminal O(3′) of the other. In the other groove, only fragments of this bridge exist, and the two links from the phosphate group hydrogen bonded to N(4) of residue C[1] are terminated after one water molecule and two water molecules (Figure 7A, top).

Generation of a Longer Parallel Homo-bcd(C) Duplex

A translation and a rotation of the repeated unit are required to generate a helix. These two parameters can be obtained from an analysis of the relative arrangement of base pairs in a dimer such as the $[bcd(C_2)]_2$ double helix (31). The selected pairs of equivalent atoms from repeated residues will determine the position of the helical axis, as well as the actual values for helical twist and rise. Table V lists the helical parameters resulting from different atom pairs (probe) for three different dimeric double helices. In the case of the $[r(AU)]_2$ duplex, the calculated helical parameters

Figure 9: Stereo diagram of a model structure for a double-stranded octamer $[bcd(C_8)]_2$, extrapolated form the $[bcd(C_2)]_2$ crystal structure. The view is across the two identical grooves with both 5′-termini at the top, and atom types are coded as in Figures 3 B,C. Note the alternating arrangement of phosphate groups within strands, which is caused by slightly different conformations of the two residues in the $bcd(C_2)$ dimer.

show only slight dependence on the chosen probe, whereas twist and rise vary considerably for the two other duplexes. Such deviations indicate geometrical heterogeneities between residues from single strands or between strands in the two latter cases. This is consistent with larger deviations for superpositions of intrastrand residues with $bcd(C_2)$, or for the superposition of strands with d(CG), compared to the RNA dimer (Table V). Consequently, the deviations between observed and generated coordinates are larger for the DNA duplexes (see helix sigma in Table V). Applying the calculated parameters to a dimer duplex and generating, for example a tetramer, will thus result in a relatively smooth, continuous duplex with the r(AU) dimer. However, from a tetramer based on the parameters of the $[bcd(C_2)]_2$ duplex, one can expect the longer fragment to be less regular, with discontinuities in the backbones.

Although the dimeric $[bcd(C_2)]_2$ fragment allows the initial analysis of the geometrical details of a parallel-stranded double helix, one may gain better insight into the topology of such an arrangement by examining a longer stretch. We therefore used the generated helix operator (probe 1, Table V) to construct an octameric $[bcd(C_8)]_2$ duplex. The resulting arrangement of dimeric units in the octamer leads to gaps of 2.8 Å between terminal 5′- and 3′-hydroxyl groups. This distance allows bridging of the two oxygens by a phosphate. However, introduction of a phosphate group leads to close contacts between one of the phosphate oxygens and hydrogens H(1′) and H(2′2) of the furanose ring from the adjacent residue (1.1 and 1.7 Å, respectively). Furthermore, the arrangement of the newly introduced phosphate group differs form the one of the phosphate group in the dimeric units, generating a *zig-zag* pattern in

the backbones. The introduced sterical strains were therefore relaxed by subjecting the constructed duplex to energy minimization using the TRIPOS force field (33). Electrostatic interactions were not taken into account during the minimization. Refinement was then performed in two steps. During the first 100 cycles, distant restraints for base pair hydrogen bonds were applied (2.8 Å, force constant 200 kcalmol^{-1}Å^{-2}). In a second stage, the duplex was refined without restraints for another 100 cycles. The energy-minimized octamer duplex is depicted in Figure 9. The diameter of the parallel-stranded duplex is about 23 Å. The two identical grooves are 9 Å wide (calculated by subtracting the van der Waals radii for phosphate groups, 5.8 Å, from distances between selected interstrand phosphate pairs) and about 6 Å deep.

Conclusions

The most prominent features of the [bcd(C_2)]$_2$ parallel-stranded double helix are: (1) Formation of hemiprotonated C-C$^+$ base pairs with three hydrogen bonds. (2) Values for helical rise and twist, which resemble those of standard B-DNA duplexes. (3) The C(1′)-*exo* and C(2′)-*endo* furanose puckers which are most commonly adopted by the deoxyriboses in B-type double helices. (4) Backbone torsion angles, with exception of β, γ and δ, which fall into the ranges observed in B-DNA. Compression of β and δ, as well as widening of γ, compared to the B-DNA backbone, are caused by the ethylene bridges between C(3′) and C(5′), generating the bicyclic sugar framework. (5) The *trans* arrangement of glycosyl bonds, leading to identical grooves and to a duplex diameter, which is similar to those of the antiparallel right-handed duplexes with purine-pyrimidine base pairs.

This crystal structure therefore provides evidence for the double stranded nature of poly(dC). An interesting conclusion may be drawn from the different environments around the two C-C$^+$ base pairs in the present structure. Hydrogen bonding of N(4) atoms to phosphate oxygens with one base pair, and hydrogen bonding of N(4) atoms to solvent molecules with the adjacent pair, could be an indication for the presence of two different C-C$^+$ base pair resonance forms in the [bcd(C_2)]$_2$ duplex. The dislocation of the positive charge to both N(4) atoms, away from the N(3) positions, in every second base pair could reduce charge-charge repulsion between adjacent hemiprotonated cytosine base pairs in C-rich stretches. Compared to the recently reported tetrameric solution structure of the DNA oligomer with sequence 5′-TCCCCC (34), the double stranded arrangement reported here displays considerably more stacking, as concluded from the greater overlap between adjacent cytosine rings. Somewhat similar to the tetrameric structure, the arrangement of carbonyl groups from stacked bases (assuming parallel relative orientations in the [bcd(C_2)]$_2$ duplex) guarantees an additional stabilizing electrostatic interaction. Together, this may account for the greater stability of C-C$^+$ base pairs compared to Watson-Crick G-C or A-T pairs (35).

The nature of the adopted structure is likely to depend on the specific sequence of the C-rich sequence under investigation. In addition to the i-motif, the C-C$^+$ base pairs containing arrangements recently reported include parallel double helices (35,36,37,38), as well as multistranded complexes (39). Furthermore, other parameters, such as pH and salt concentrations, will influence the conformation adopted by

regions with high cytosine content. Only very limited conclusions concerning the structure of poly(C) can be made based on the structure reported here. Provided a parallel double helical arrangement exists, the different pucker of riboses in RNA must clearly produce a structure which differs considerably from a structure with B-DNA like features of the backbones, such as the $[bcd(C_2)]_2$ duplex. This is consistent with dramatic differences between the pK values of poly(dC) (7.4; (40)) and poly(C) (5.7; (41)). Moreover, the proposed structures for poly(C) exhibit great variations, and include double- (42,43), as well as single-stranded models (44).

References and Footnotes

1. Zamecnik, P.C. and Stephenson, M.L., *Proc. Natl. Acad. Sci. U.S.A. 75*, 280-284 (1978). *ibid. Proc. Natl. Acad. Sci. U.S.A. 75*, 285-290 (1978).
2. Uhlmann, E. and Peyman, A., *Chem. Rev. 90*, 543-584 (1990).
3. Miller, P.S., Agris, C.H., Aurelian, L., Blake, K.R., Murakami, A., Reddy, M.P., Spitz, S.A. and Ts'o, P.O.P., *Biochimie 67*, 769-776 (1985).
4. Eckstein, F., *Annu. Rev. Biochem. 54*, 367-402 (1985).
5. Bannwarth, W., *Helv. Chim. Acta 71*, 1517-1527 (1988).
6. Bloch, E., Lavignon, M., Bertrand, J.-R., Pognan, F., Morvan, F., Malvy, C., Rayner, B., Imbach, J.-L. and Paoletti, C., *Gene 72*, 349-360 (1988).
7. Nielsen, P.E., Egholm, M., Berg, R.H. and Buchardt, O., *Science 254*, 1497-1500 (1991).
8. Eschenmoser, A. and Loewenthal, E., *Chem. Soc. Rev. 21*, 1-16 (1992).
9. Hunziker, J., Roth, H.-J., Böhringer, M., Giger, A., Diederichsen, U., Göbel, M., Krishnan, R., Jaun, B., Leumann, C. and Eschenmoser, A., *Helv. Chim. Acta 76*, 259-352 (1993).
10. Tarköy, M., Bolli, M., Schweizer, B. and Leumann, C., *Helv. Chim. Acta 76*, 481-510 (1993).
11. Tarköy, M. and Leumann, C., *Angew. Chem. 105*, 1516-1518 (1993). *ibid. Angew. Chem. Int. Ed. Engl. 32*, 1432-1434 (1993).
12. Tarköy, M., *ETH-Dissertation*, Nr. 10109 (1993).
13. Egli, M., Lubini, P., Bolli, M., Dobler, M. and Leumann, C., *J. Am. Chem. Soc. 115*, 5855-5856 (1993).
14. Bolli, M. and Leumann, C., unpublished work (1993).
15. Sheldrick, G.M., in *Crystallographic Computing 3* (Sheldrick, G. M., Krüger, C. and Goddard, T., Eds.) Oxford Univ. Press, Oxford, pp. 175-189 (1986).
16. Maverick, E., *Bigshelx-76*, Univ. of California, Los Angeles (1985).
17. Sheldrick, G.M., *Shelxl-92* Beta version, Univ. of Göttingen, Göttingen (1992).
18. CCP4 The SERC (UK) *Collaborative Computing Project No. 4*, Daresbury Laboratory, Warrington WA4 4AD, UK (1979).
19. Sack, J.S., *Chain* - a crystallographic modeling program, *J. Mol. Graphics 6*, 244-245 (1988).
20. Dickerson, R.E. *et al., Nucleic Acids Res. 17*, 1797-1803 (1989).
21. Seeman, N.C., Rosenberg, J.M., Suddath, F.L., Kim Park, J.J. and Rich, A., *J. Mol. Biol. 104*, 109-144 (1976).
22. Rosenberg, J.M., Seeman, N.C., Day, R.O. and Rich, A., *J. Mol. Biol. 104*, 145-167 (1976).
23. Westhof, E., *Nature 258*, 459-460 (1992).
24. Taylor, R. and Kennard, O., *J. Mol. Struct. 78*, 1-28 (1982).
25. Coll, M., Solans, X., Font-Alaba, M. and Subirana, J.A., *J. Biomol. Struct. Dyn. 4*, 797-811 (1987).
26. Dickerson, R.E. and Drew, H.R., *J. Mol. Biol. 149*, 761-786 (1981).
27. Kabsch, W., *Acta Crystallogr. A34*, 827-828 (1978).
28. Tong, L. and Rossmann, M.G., *Acta Cryst. A46*, 783-792 (1990).
29. Rossman, M.G. and Blow, D., *Acta Cryst. 15*, 24-31 (1962).
30. Cruse, W.B.T., Egert, E., Kennard, O., Sala, G.B., Salisbury, S.A. and Viswamitra, M.A., *Biochemistry 22*, 1833-1839 (1983).
31. Rosenberg, J.M., Seeman, N.C., Day, R.O. and Rich, A., *Biochem. Biophys. Res. Comm. 69*, 979-987 (1976).
32. Rosenberg, J.M., Seeman, N.C., Kim Park, J.J., Suddath, F.L., Nicholas, H.B. and Rich, A., *Nature 243*, 150-154 (1973).

33. Clark, M., Cramer III, R. D. and Van Opdenbosch, N., *J. Comp. Chem. 10*, 982-1012 (1989).
34. Gehring, K., Leroy, J.-L. and Guéron, M., *Nature 363*, 561-565 (1993).
35. Pilch, D.S. and Shafer, R.H., *J. Am. Chem. Soc. 115*, 2565-2571 (1993).
36. Sarma, M.H., Gupta, G. and Sarma, R.H., *FEBS lett. 205*, 223-229 (1986).
37. Luo, J., Sarma, M.H., Yuan, R. and Sarma, R.H., *FEBS lett. 306*, 223-228 (1992).
38. Robinson, H., van der Marel, G.A., van Boom, J.H. and Wang, A.H.-J., *Biochemistry 31*, 10510-10517 (1992).
39. Edwards, E.L., Patrick, M.H., Ratliff, R.L. and Gray, D.M., *Biochemistry 29*, 828-836 (1990).
40. Inman, R.B., *J. Mol. Biol. 9*, 624-637 (1964).
41. Hartman, Jr., K.A. and Rich, A., *J. Am. Chem. Soc. 87*, 2033-2039 (1965).
42. Akinrimisi, E.O., Sander, C. and Ts'o, P.O.P., *Biochemistry 2*, 340-344 (1963).
43. Langridge, R. and Rich, A., *Nature 198*, 725-728 (1963).
44. Arnott, S., Chandrasekaran, R. and Leslie, A.G.W., *J. Mol. Biol. 106*, 735-748 (1976).